Revising Fourier-transform infrared (FT-IR) and Raman spectroscopy towards brain cancer detection

Taha Lilo[a,b,*], Camilo L. M. Morais[b] ,Cationa Shenton[a] , Arup Ray[a] , and Nihal Gurusinghe[a,b].

a. Department of Neurosurgery, Royal Preston Hospital, Lancashire Teaching Hospitals NHS Trust, Preston PR2 9HT, UK.
b. School of Pharmacy and Biomedical Sciences, University of Central Lancashire, Preston PR1 2HE, UK.

***Corresponding author:** Dr. Taha Lilo, Department of Neurosurgery, Royal Preston Hospital, Lancashire Teaching Hospitals NHS Trust, Preston PR2 9HT, UK. Email: taha.lilo@icloud.com

Abstract

Fourier-transform infrared (FT-IR) and Raman spectroscopy are being widely used as sensor-based techniques towards oncology applications, in particular, to diagnose brain cancers and their subtypes due to their critical severity. Overtime these techniques became more sensitive and nowadays accuracies over 90% can be observed in several studies. This is a good indication of their potential for real clinical implementation. Herein, we present a min-review by revisiting some fundamentals of FT-IR and Raman spectroscopy along with their applications towards brain cancer detection in the literature.

Keywords: brain cancer; glioma; meningioma; glioblastoma; FT-IR; infrared spectroscopy; Raman.

1. Introduction

1.1 Brief history of Fourier-transform infrared (FT-IR) spectroscopy

Infrared (IR) spectroscopy is a vibrational spectroscopy technique used to assess the chemical composition of a sample [1]. It is based on the absorption of infrared light by the molecules that compose the material, where all molecules with a resultant dipole moment different from zero will absorb infrared radiation. The scientific idea behind the Fourier-transform infrared (FT-IR) spectroscopy was first initiated in the late 1880s by Albert A. Michelson. The founder invented an interferometer, a device that Albert and Morley used to perform famous experiments determined to measure the exact speed of light. Besides the Michelson interferometer, he also introduced the scientific optical instruments. His efforts were widely accepted and appreciated by the scientists of the day. Later in 1907, Michelson's efforts and inventions were still applicable and won the Nobel Prize in Physics.

Michelson knew the spectroscopic potential of his interferometer, although it lacked the sensitive detectors and the Fourier-transform algorithms that consequently barred the instrument from its practical application. However, he still manipulated and used it to solve many doublet spectra back then in the field [2]. There were quite many challenges that scientists faced while using Fourier-transform spectroscopy (FTS) to compute the Fourier-transform of interferograms. It is because the FTS was not able to directly invert the values, so they guessed some spectra, calculated the inverse of their Fourier-transform, and then compared it to the interferogram they had earlier measured. The best results were obtained after modifying the guessed spectra to match the data at hand.

It is in the late 1940s that the practical application of the FTS was considered useful. The scientists first used the interferograms when measuring light from the celestial bodies after producing the first Fourier-transform spectrum in 1949. At this point, it became more accessible for the scientists to calculate the continuous necessary Fourier transforms though it became a task that was so difficult and consumed much time. Here, the scientists introduced the lamellar granting and the Fabry-Perot interferometers, besides the Michelson's. The schematic Figure 1a below represents the basic Michelson interferometer.

Movasaghi *et al.* (2008) [3] speculated that the lamellar granting spectrometer share many standard features with the Michelson's. These two beam and multicomplex devices have high optical ability to produce the interferograms, which, when Fourier-transformed, provide the desired spectrum. However, in the lamellar granting instrument, the optical modulation part constitutes a pair of mirrors that are arranged in a tongue and groove manner to bring the appearance of one large mirror divided into two or more horizontal strips as indicated in Figure 1b.

Through the Fresnel mirrors, the scientists could observe interferences with the blue-ray path difference near line F at wavelength 1737. After the reflection on both mirror surfaces on the thin plate, they noticed increased interference at wavelength 3406. Later, they perfected the technique and used it to detect IR radiations and to measure IR wavelengths. The lamellar granting interferometer is preferred to Michelson's because it uses the entire wavefront, unlike the Michelson's that loses one half of the total flux even when the beam splitter is perfect and efficient. Additionally, the lamellar granting interferometer has high efficiency due to its far-infrared region.

The increased interest in spectroscopy facilitated advancements in interferometers and its applications in physical systems. The improvements in the theories included the fast Fourier-transform algorithm that made the electronic computing of the Fourier transforms easy and efficient [4]. The idea substantially reduced the time of calculations and magnitude orders, as well as turning the interferogram to a readable spectrum feasible. The Fourier spectroscopy generated a new weapon to greater effectiveness to experimentalists in 1969.

The IR technique applied a reliable, simple, powerful, and most effective method to analyse organic materials with a dispersive technology in the early 1940s. However, there were shortcomings attached to its scanning speed and the general manual operations; it was too slow. The wavelength of the light that passed through also measured one by one with just a slit controlling the spectral bandwidth. The dispersive spectrometer required a source of visible wavelength calibrations because there was no reference to any. The dispersive spectrometer is shown in Figure 1c.

These shortcomings enhanced further improvements on the dispersive. Consequently, the improved phase came handy with three significant advantages over the dispersive FT-IR system. The modern FT-IR spectrometer does not separate light into individual frequencies for measurements; instead, every interferogram has information from each wavelength of the light being measured [5]. Through the interferometer, the FT-IR spectrometer modulates the wavelength from the broadband infrared source. The detector then measures the intensity of the transmitted and reflected light as a function of its wavelength.

With increased technology, modern spectrometers availability and enhanced capabilities increased with a gradual reduction in costs. Currently, the FTS hastened by the fastest computers

processes the Fourier transformations with visible, infrared, and microwave regions in microseconds and are conventional devices in laboratories worldwide. The increase of performance and reduction in cost make FTS an attractive spectroscopy tool in many disciplines. Therefore, Fourier spectroscopy is a collective term that has been used while describing the breakdown of varying signals into the respective frequency components. It entails compelling mathematical methods that have been used by a series of spectroscopies, including the Fourier-transform infrared (FT-IR), Fourier-transform near infrared (FT-NIR), and Fourier-transform Raman spectroscopy.

1.2 Brief history of Raman spectroscopy

On the other hand, Raman spectroscopy, a technique introduced in 1928 by Sir Chandrasekhara Venkata Raman, explained the effects of light changing its wavelength when it is passing through a transparent object. In his experiment, the Indian Physicist used sunlight as a source, liquid in a bucket as the collector, and his eyes, detectors. This remarkable phenomenon was called the Raman scattering. He gradually improved his instrumentation to achieve a better result; from helium, argon, rubidium and cesium lamps to lasers Ar^+ (351.l-514.5 nm), Kr^+ (337.4-676.4 nm) and today laser diodes NdYAG (1,064 nm) while the photomultipliers and CCD cameras used as detectors. Moreover, the extended the progress to the detection systems from the cooled cascade RCA IP21 in 1942 to cooled RCA C-7073B photomultiplier in 1950 then cooled RCA IP21 photomultiplier tube that was used by 1953 [6]. In the meantime, it was introduced a device called Hilger E612 that was used as a photoelectric instrument. Subsequently, Cary Model 81 Raman spectrometer came to existence. It used a three kilowatts helicon Hg arc of Toronto type with double gating, double slit twin monochromator.

The persistence in developing the optical system continued in 1960. The scientists learned that a twin monochromator could eliminate the stray lights more efficiently compared to the single monochromator. Instead, they introduced a triple monochromator, which was perfect in removing the stray gleams. Eventually, in 1968, the Holographic gratings appeared, which wholesomely improved the efficiency of the Raman scattering and collection systems. The developments have ensured the current commercial state of the art of the Raman measurements and instrumentation.

Typically, the Raman scattering is used to collect spectroscopic data through an inelastic scattering process based on molecular polarizability changes [7]. Inelastic scattering involves the frequency of changes that occur in the monochromatic photons in the light after interacting with samples. The electromagnetic scattering occurs due to vibrations and rotations between the molecules. The real photons have varied energy, therefore the scattering system is likely to lose or gain power. The difference in the frequency of incoming and outgoing photons forms Stokes and anti-Stokes scattering, as shown in Figure 2.

2. Spectral features

Both FT-IR and Raman spectroscopy can be employed in chemical analysis of various substances, where signals of vibrational modes for the molecules bonds that compose the material are obtained. These unique spectral features for FT-IR and Raman make these spectroscopy techniques very attractive to determine chemical compositions of unknown substances.

2.1 Fourier-transform infrared (FT-IR) spectroscopy

FT-IR has been widely used to help analysts deeply understand materials and products through analytical testing. FT-IR can be employed in the sample through transmission, reflectance or transflectance, and the spectral data acquired are used to assist in the identification of the sample chemical composition. This technique can be applied to investigate a wide range of materials, from paints, foods, pharmaceuticals, polymers to biological-derived samples, such as tissue and biofluids [8].

FT-IR can be used in both qualitative and quantitative analysis of organic and inorganic materials. It records a spectrochemical information composed of the absorption intensities for each wavenumber of mid-infrared spectrum (4,000–400 cm^{-1}). The infrared bands carry vibrational information used to identify the molecular components and their respective structures; thus the spectra generate a distinctive molecular fingerprint used to screen and scan samples in various segments. The fingerprint spectrum for biological samples, also called the "biofingerprint" region, ranges from 1,800–900 cm^{-1} and contains information of key biomolecules such as lipids, proteins, carbohydrates and nucleic acids [9] (Figure 3a). Changes in the IR signature for these biomolecules are associated with concentration changes (changes of band intensity) and changes of molecular configuration and neighboring functional groups (band shifts towards higher or lower wavenumbers).

2.1 Raman spectroscopy

Raman is a spectroscopy technique that, similarly to FT-IR, is used to obtain vibrational spectrochemical information of a sample. Raman is complementary to FT-IR, being associated with molecular polarizability changes while the latter is associated with changes in molecular dipole moments. Since the anti-Stokes scattering is less often at room temperature, the Raman

spectrum recorded and analysed by spectrometers is generally the Stokes scattering, whose Raman shift commonly varies from 0 to 4,000 cm^{-1} [10].

Raman is often used to analyse biological samples, since it is water transparent, that is, the water signal in Raman is very small so not masking the signal from the other chemical compounds below 3000 cm^{-1} [1]. IR is sensitive to water, therefore samples are often measured dry in IR spectroscopy to minimise the water interference; while Raman allow measuring samples at all forms, including liquids or dry samples [11]. The Raman biofingerprint region is between 2000–500 cm^{-1}, and comprises mostly stretching vibrations for carbohydrates, lipids, proteins and nucleic acids (Figure 3b) [9].

In the Raman instrumentation, the monochromatic laser light is shone on the sample. The sample can be measured with no prior preparation, or it may also be mixed with nanoparticles; coated with a transparent layer that is non-reactive to the Raman laser, like the SiO2; or by placing it in DI water to prevent stray lighting [13]. The electromagnetic radiation that contains the near-infrared, visible, or the ultraviolet range that is emitted from the sample is then filtered out. The filtration can be done through the notch or the band pass filters, and then the resulting infrared light passes through the monochromator and finally to the CCD detectors.

In Raman microspectroscopy, light is let through the microscope before it reaches the sample. This allows the light to focus on a smaller area of 1 μm^2 for accurate mapping of a particular example through a confocal microscopy [14]. However, precautions should be taken when mapping the sample to avoid its destruction by the concentrated laser light on each sample spot.

3. Differences between FT-IR and Raman spectroscopy

FT-IR and Raman are complementary spectroscopic techniques that are based on molecular vibration signatures. Although these similarities, there are direct points that distinguish the origin, functionality, and the mode of identification of unknown materials by the two techniques [15]. By principle, as mentioned earlier, FT-IR is based on changes of dipole moment while Raman in changes of molecular polarizability, hence, the spectral profile for a same sample measured by both techniques will be substantially different, where signatures will be present at specific wavenumber positions in the FT-IR spectrum while not in the Raman spectrum or vice-versa. Additionally, from a practical point-of-view, these techniques considerably diverge. FT-IR is a more robust technique with less physical interfering however not as sensitive as Raman spectroscopy to analyse certain compounds, such as inorganic substances. Also, FT-IR is greatly affected by water absorption. On the other hand, Raman is water-free and is a powerful technique to analyse inorganic substances, such as silica crystals and carbon nanotubes. However, Raman is highly affected by cosmic rays and fluorescence interfering which can mask the signal of interest. The latter is especially apparent when analysing coloured substances, hence, making it difficult to analyse these types of substances with Raman. In addition, when the biological sample is exposed to high-energy laser sources or prolonged exposure time, Raman may be destructive to the sample [11]. Table 1 summarises the main differences between the two spectroscopic techniques.

4. Clinical implications

Brain cancers are one of the main causes of cancer-related deaths worldwide, accounting to 3% of all tumours diagnosed annually and with an increasing incidence rate over the last years [16]. They are difficult to be fully removed thus causing post-surgery consequences and likely reoccurrence which increases mortally, even though they comprise a small portion of all tumours often diagnosed [16, 17]. Most of brain cancers are either meningiomas or gliomas tumours [18]. Meningiomas are less aggressive types of tumours, often benign, that occurs in a supratentorial location, such as towards the spinal cord or the meninges surrounding the brain [19-21]. Gliomas, on the other hand, are a more aggressive type, comprising neuroepithelial tumours originating from the glial or supporting cells of the central nervous system (CNS) [22].

FT-IR spectroscopy, as well as other molecular spectroscopy techniques such as liquid chromatography-mass spectrometry (LC/MS), nuclear magnetic resonance (NMR) spectroscopy, near-infrared (NIR), and Raman spectroscopy often compose a benchmark to provide robust and supportive data about the sample chemical composition. FT-IR and Raman spectroscopy are a fast, low-cost, and reagent-free tool for cancer diagnostic [23]. They are high throughput techniques which, together with multivariate analysis or machine learning algorithms, can be used for cancer detection in an automatic, quick and easy fashion [24]. For brain cancers specifically, knowing the tumour type or subtype is essential to start the correct patient treatment and reduce post-surgery risks [21, 23], which ultimately will decrease its mortality.

Brain cancers are traditionally detected by using a combination of techniques, such as imaging tests by means of magnetic resonance imaging (MRI), computed tomography (CT) or positron emission tomography (PET) scans to detect abnormal areas [25], together with tissue biopsies to identify the tumour type and grade by means of histopathology techniques [26]. These techniques show some disadvantages in comparison with FT-IR and Raman spectroscopy. Imaging

tests such as MRI, CT and PET scans require expensive instrumentation in comparison with FT-IR and Raman spectroscopy techniques, thus they are not widely available in some areas, especially in developing regions. Biopsies are minor surgeries that may bring much discomfort to patients and their histological analyses are laborious, complex and can be analyst-dependent. Furthermore, these traditional methods for tumour detection are much slower when compared to spectroscopy techniques, where the results from this latter can be obtained within seconds through machine learning techniques. Furthermore, FT-IR and Raman spectroscopy are an objective technique, where the results are only dependent on the sample chemical composition; and these spectroscopy techniques are much less-invasive than the traditional methods, where, for example, biofluids instead of tissue biopsies can be used for brain cancers diagnosis [27, 28].

Several studies have used FT-IR or Raman spectroscopy to investigate biological samples, either tissues or biofluids, to detect brain cancers and their subtypes. For example, Qu *et al.* [29] used FT-IR spectroscopy for rapid diagnosis of gliomas based on serum samples; Fabelo *et al.* [30] used FT-IR spectroscopy to detect brain tumour tissue samples; Depciuch *et al.* [31] used FT-IR and Raman spectroscopy to detect glioblastoma in tissue samples; Kopec *et al.* [32] used Raman imaging to detect various types of human brain tumours; Riva *et al.* [33] used Raman spectroscopy to detect gliomas based on fresh tissue samples; Zhang *et al.* [34] used Raman spectroscopy to detect gliomas based on serum samples; and, Galli *et al.* [35] used Raman spectroscopy to detect brain cancers in tumour biopsies.

Cancers are caused by changes in the biochemical pathways undergoing in our bodies due to a series of factors for which their occurrence and mechanism remains very complex [36]. Alterations in the cellular energy metabolism is an important process that occur during the transition from normal to cancer cells and it is highly entwined to cell proliferation and cell death

[37]. For example, the activation of the polyamine metabolism is closely related with cellular proliferation [38]. Brain cancers show particular complexity despite some advances in discovering genetic and molecular features about this pathology [39], as an example, the chromosome complete or partial loss of the tumour suppression gene or enzymes associated to various signaling mechanism for the cell cycle control [40]. Several studies using both FT-IR and Raman spectroscopy have found spectral markers associated with tumour appearance and progression, as listed in Tables 2 and 3. These markers are molecular fragments directly related to the sample biochemical composition thus reflecting the patient status on the time of measurement, therefore, covering biochemical signatures related to the tumour itself or the system response. This spectral information acquired from FT-IR and Raman spectroscopy combined with data from other techniques, such as mass spectrometry, could be used to identify the real biomarkers associated to the disease. Table 4 summarizes their main findings along with the classification algorithms used to distinguish the samples.

The classification performance to distinguish non-cancer from cancer samples or cancer subtypes seems to improve overtime. The results are dependent on the instrumentation, sample type and preparation and the algorithm used to process the spectral data. The results also look more promising when using mapping or imaging techniques instead of point-spectra, since spatially-distributed information carry more information about the sample specimen and often improves the classification [59, 60]. Also, the analyses were made using different algorithms which have weight in the classification outcomes. Often PCA-LDA (or just LDA), PLS-DA and SVM are used to discriminate and classify the samples. In PCA, the pre-processed data are decomposed into a few numbers of factors called Principal Components (PCs) responsible for most of the variance within the original dataset [61]. The PCs are orthogonal to each other and are built in a decreasing order

of explained variance, so that the first PC explains most of the variance, followed by the second PC and so on. Each PC is composed of scores, representing the variance on the sample direction, and loadings, representing the variance on the wavenumber direction. The scores can be used to identify similarities/dissimilarities between the samples through the visualisation of clustering patterns, while the loadings can be used to discover the wavenumbers of highest importance responsible for clustering segregation [24]. LDA can be applied to the PCA scores in order to classify the samples based on a Mahalanobis distance calculation [62].

PLS-DA is a supervised feature extraction and classification algorithm where partial least squares (PLS) is applied to the pre-processed spectral data reducing the original wavenumbers to a small number of latent variables (LVs). Then, a linear discriminant classifier is used for classifying the groups [63]. PLS-DA usually performs better than PCA-LDA, therefore it is commonly employed as a benchmark technique for spectral classification [64]. SVM works firstly by transforming the data space into a feature space by means of a kernel function which is often non-linear. Then, a linear decision boundary is fit between the closest samples to the border of each class (these samples are called support vectors), hence classifying the samples according to this boundary [24, 64].

These algorithms are applied after pre-processing the samples spectra, where peak removal (*e.g.*, cosmic rays removal in Raman spectroscopy), selection of specific spectral regions of interest (*e.g.*, biofingerprint region), smoothing, baseline corrections, derivatives, and normalisation procedures are performed to reduce spectral interferences and improve the signal-to-noise ratio of the spectra [24, 65]. The final classification is then made by these machine learning algorithms where a training set of samples feeds the model while a test set validates them towards external samples prediction [24]. It is important to test different types of algorithms since results may vary

depending on the algorithm chosen, and validated them by cross-validation and external predictions in order to avoid overfitting, which may lead to false results [24].

Figure 4 shows a flowchart with the steps one may perform to analyse brain cancer samples using either FT-IR or Raman spectroscopy techniques. For each step there are key points to be considered. For the sample preparation, first the type of sample must be defined: biofluids, such as blood serum, plasma, urine; or, tissue samples. Some biofluids need further preparation such as unthawing (if the samples are frozen), drying to avoid water interference if the sample is going to be analysed by FT-IR and centrifugation if the sample contains suspended matter [45]. For tissue samples, the tissue type (fresh, snap-frozen, FFPE) should be considered. Fresh tissue tends to degrade quickly, while snap-frozen may bring water inference for FT-IR and FFPE brings paraffin interference [8, 11]. De-parafinisation of FFPE tissues is a common practice to be performed [45].

During spectral acquisition, the acquisition mode is an important aspect and it will change according to the application purpose. For analysis of solid and dried liquid samples using FT-IR spectroscopy, the use of ATR module is a good option to maximise the signal-to-noise ratio [8]. If the equipment is equipped with an imaging apparatus, hyperspectral can also be acquired. The spectral resolution is recommend being set in between 4 to 8 cm^{-1} and the wavenumber range in between 400 to 4000 cm^{-1} [45]. Changes of resolution and wavenumber range may speed the spectral acquisition, but may hide important spectral information. It is also important to set correct parameters for the Raman laser source in order to avoid damage to sample while keeping a good signal-to-noise ratio [11]. In addition, spectral interferences during Raman acquisition such as fluorescence, signal saturation and cosmic rays should be observed and preferably corrected during sample acquisition. Furthermore, the file extension in which the data is saved is important. One should make sure the files are saved in a format readable by the data analysis software [24].

For the data analysis, usually the first step is to pre-process the spectra in order to minimise interferences [24]. Following pre-processing, exploratory analysis by means of PCA and HCA algorithms can be performed. To build supervised classification models, the data must be split into at least training and test sets [66]. The training set is used for model construction while the test set for model validation. There are several algorithms for classification, such as LDA, QDA, PLS-DA and SVM, which can be used in conjunction with PCA [24]. Feature extraction and selection can also be performed with the spectral data in order to identify important wavenumbers related to class separation. Some techniques include the visual analysis of the difference-between-mean (DBM) spectra, PCA loadings, PLS-DA regression coefficients, and, the successive projections algorithm (SPA) and genetic algorithms (GA) selected variables [24]. Lastly, the model must be validated with blind test samples where parameters such as accuracy, sensitivity and specificity are calculation, in addition to statistical test, such as p-values test, to verify the selected wavenumbers related to class differentiation.

5. Conclusion

Improvements of FT-IR and Raman instrumentation overtime have finally put them in the lead through their improved spectral quality, reproducibility of data, and user-friendliness coupled with relatively reduced maintenance cost. Advancements of Raman and FT-IR spectroscopy have positively influenced the health sector to industrial and point-of-care applications. The real time application and the flexibility in the rapidly growing lasers and detectors have further offered the unique strengths in the existing diagnostic devices.

Both FT-IR and Raman generate chemically-rich spectral signatures of tissue or biofluids that can be used for a wide range of clinical applications, especially towards oncology. For brain cancers, these techniques have proved to be of great potential to detect them and their subtypes. Moving forward, the industrial production of lower-cost, sensitive and more modern devices are crucial for bringing these technologies into the clinical theatres as complementary tools to aid diagnostic. This in effect will reduce the death rates seen in the world today and it will also give timely and permanent solutions to chronic disease.

Conflict of Interest

The authors have no conflicts of interest to declare.

References

[1] D.A. Skoog, F.J. Holler, S.R. Crouch, Principles of Instrumental Analysis, sixth ed., Thomson Brooks/Cole, Belmont, 2007.

[2] N. Navas, J. Romero-Pastor, E. Manzano, C. Cardell, Benefits of applying combined diffuse reflectance FTIR spectroscopy and principal component analysis for the study of blue tempera historical painting, Anal. Chim. Acta 630 (2008) 141–149. https://doi.org/10.1016/j.aca.2008.10.008

[3] Z. Movasaghi, S. Rehman, I. ur Rehman, Fourier Transform Infrared (FTIR) Spectroscopy of Biological Tissues, Appl. Spectrosc. Rev. 43 (2008) 134–179. https://doi.org/10.1080/05704920701829043

[4] D.M. Livingston, The master of light: a biography of Albert A. Michelson, University of Chicago Press, Chicago, 1973.

[5] S. Duraipandian, W. Zheng, J. Ng, J.J.H. Low, A. Ilancheran, Z. Huang, Near-infrared-excited confocal Raman spectroscopy advances in vivo diagnosis of cervical precancer, J. Biomed. Opt. 18 (2013) 067007. https://doi.org/10.1117/1.JBO.18.6.067007

[6] P. Vandenabeele, H. Edwards, Raman Spectroscopy in Archaeology and Art History: Volume 2, Royal Society of Chemistry, London, 2018.

[7] M.C.D. Santos, C.L.M. Morais, Y.M. Nascimento, J.M.G. Araujo, K.M.G. Lima, Spectroscopy with computational analysis in virological studies: A decade (2006–2016), Trends Anal. Chem. 97 (2017) 244–256. https://doi.org/10.1016/j.trac.2017.09.015

[8] M.J. Baker, J. Trevisan, P. Bassan, R. Bhargava, H.J. Butler, K.M. Dorling, P.R. Fielden, S.W. Fogarty, N.J. Fullwood, K.A. Heys, C. Hughes, P. Lasch, P.L. Martin-Hirsch, B. Obinaju, G.D. Sockalingum, J. Sulé-Suso, R.J. Strong, M.J. Walsh, B.R. Wood, P. Gardner, F.L. Martin, Using Fourier transform IR spectroscopy to analyze biological materials, Nat. Protoc. 9 (2014) 1771–1791. https://doi.org/10.1038/nprot.2014.110

[9] J.G. Kelly, J. Trevisan, A.D. Scott, P.L. Carmichael, H.M. Pollock, P.L. Martin-Hirsch, F.L. Martin, Biospectroscopy to metabolically profile biomolecular structure: a multistage approach linking computational analysis with biomarkers, J. Proteome Res. 10 (2011) 1437–1448. https://doi.org/10.1021/pr101067u

[10] C.L.M. Morais, T. Lilo, K.M. Ashton, C. Davis, T.P. Dawson, N. Gurusinghe, F.L. Martin, Determination of meningioma brain tumour grades using Raman microspectroscopy imaging, Analyst 144 (2019) 7024–7031. https://doi.org/10.1039/C9AN01551E

[11] H.J. Butler, L. Ashton, B. Bird, G. Cinque, K. Curtis, J. Dorney, K. Esmonde-White, N.J. Fullwood, B. Gardner, P.L. Martin-Hirsch, M.J. Walsh, M.R. McAinsh, N. Stone, F.L. Martin, Using Raman spectroscopy to characterize biological materials, Nat. Protoc. 11 (2016) 664–687. https://doi.org/10.1038/nprot.2016.036

[12] Z. Movasaghi, S. Rehman, I.U. Rehman, Raman Spectroscopy of Biological Tissues, Appl. Spectrosc. Rev. 42 (2007) 493–541. https://doi.org/10.1080/05704920701551530

[13] R.J. Meilunas, J.G. Bentsen, A. Steinberg, Analysis of aged paint binders by FTIR spectroscopy, Stud. Conserv. 35 (1990) 33–51. https://doi.org/10.2307/1506280

[14] R.M. Stöckle, Y.D. Suh, V. Deckert, R. Zenobi, Nanoscale chemical analysis by tip-enhanced Raman spectroscopy, Chem. Phys. Lett. 318 (2000) 131–136. https://doi.org/10.1016/S0009-2614(99)01451-7

[15] M. Poletto, A.J. Zattera, R.M.C. Santana, Structural differences between wood species: Evidence from chemical composition, FTIR spectroscopy, and thermogravimetric analysis, J. Appl. Polym. Sci. 126 (2012) E337–E344. https://doi.org/10.1002/app.36991

[16] D. Bury, C.L.M. Morais, F.L. Martin, K.M.G. Lima, K.M. Ashton, M.J. Baker, T.P. Dawson, Discrimination of fresh frozen non-tumour and tumour brain tissue using spectrochemical analyses and a classification model, Br. J. Neurosurg. 34 (2020) 40–45. https://doi.org/10.1080/02688697.2019.1679352

[17] T. Hollon, S. Lewis, C.W. Freudiger, X.S. Xie, D.A. Orringer, Improving the accuracy of brain tumor surgery via Raman-based technology, Neurosurg. Focus 40 (2016) E9. https://doi.org/10.3171/2015.12.FOCUS15557

[18] K. Gajjar, L.D. Heppenstall, W. Pang, K.M. Ashton, J. Trevisan, I.I. Patel, V. Llabjani, H.F. Stringfellow, P.L. Martin-Hirsch, T. Dawson, F.L. Martin, Diagnostic segregation of human brain tumours using Fourier-transform infrared and/or Raman spectroscopy coupled with discriminant analysis, Anal. Methods 5 (2013) 89–102. https://doi.org/10.1039/C2AY25544H

[19] K. Huntoon, A.M.S. Toland, S. Dahiya, Meningioma: A Review of Clinicopathological and Molecular Aspects, Front. Oncol. 10 (2020) 579599. https://doi.org/10.3389/fonc.2020.579599

[20] K. Mehta, A. Atak, A. Sahu, S. Srivastava, M. Krishna C, An early investigative serum Raman spectroscopy study of meningioma, Analyst 143 (2018) 1916–1923. https://doi.org/10.1039/C8AN00224J

[21] T. Lilo, C.L.M. Morais, K.M. Ashton, A. Pardilho, C. Davis, T.P. Dawson, N. Gurusinghe, F.L. Martin, Spectrochemical differentiation of meningioma tumours based on attenuated total reflection Fourier-transform infrared (ATR-FTIR) spectroscopy, Anal. Bioanal. Chem. 412 (2020) 1077–1086. https://doi.org/10.1007/s00216-019-02332-w

[22] M.E. Davis, Epidemiology and Overview of Gliomas, Semin. Oncol. Nurs. 34 (2018) 420–429. https://doi.org/10.1016/j.soncn.2018.10.001

[23] D. Bury, C.L.M. Morais, M. Paraskevaidi, K.M. Ashton, T.P. Dawson, F.L. Martin, Spectral classification for diagnosis involving numerous pathologies in a complex clinical setting: A neuro-oncology example, Spectrochim. Acta A Mol. Biomol. Spectrosc. 206 (2019) 89–96. https://doi.org/10.1016/j.saa.2018.07.078

[24] C.L.M. Morais, K.M.G. Lima, M. Singh, F.L. Martin, Tutorial: multivariate classification for vibrational spectroscopy in biological samples, Nat. Protoc. 15 (2020) 2143–2162. https://doi.org/10.1038/s41596-020-0322-8

[25] A.S. Peddinti, S. Maloji, K. Manepalli, Evolution in diagnosis and detection of brain tumor – review, J. Phys.: Conf. Ser. 2115 (2021) 012039. https://doi.org/10.1088/1742-6596/2115/1/012039

[26] G.S. Tandel, M. Biswas, O.G. Kakde, A. Tiwari, H.S. Suri, M. Turk, J.R. Laird, C.K. Asare, A.A. Ankrah, N.N. Khanna, B.K. Madhusudhan, L. Saba, J.S. Suri, A Review on a Deep

Learning Perspective in Brain Cancer Classification, Cancers 11 (2019) 111. https://doi.org/10.3390/cancers11010111

[27] A.G. Theakstone, P.M. Brennan, M.D. Jenkinson, S.J. Mills, K. Syed, C. Rinaldi, Y. Xu, R. Goodacre, H.J. Butler, D.S. Palmer, B.R. Smith, M.J. Baker, Rapid Spectroscopic Liquid Biopsy for the Universal Detection of Brain Tumours, Cancers 13 (2021) 3851. https://doi.org/10.3390/cancers13153851

[28] A. Sala, D.J. Anderson, P.M. Brennan, H.J. Butler, J.M. Cameron, M.D. Jenkinson, C. Rinaldi, A.G. Theakstone, M.J. Baker, Biofluid diagnostics by FTIR spectroscopy: A platform technology for cancer detection, Cancer Lett. 477 (2020) 122–130. https://doi.org/10.1016/j.canlet.2020.02.020

[29] H. Qu, W. Wu, C. Chen, Z. Yan, W. Guo, C. Meng, X. Lv, F. Chen, C. Chen, Application of serum mid-infrared spectroscopy combined with an ensemble learning method in rapid diagnosis of gliomas, Anal. Methods 13 (2021) 4642–4651. https://doi.org/10.1039/D1AY00802A

[30] H. Fabelo, S. Ortega, E. Casselden, J. Loh, H. Bulstrode, A. Zolnourian, P. Grundy, G.M. Callico, D. Bulters, R. Sarmiento, SVM Optimization for Brain Tumor Identification Using Infrared Spectroscopic Samples, Sensors 18 (2018) 4487. https://doi.org/10.3390/s18124487

[31] J. Depciuch, B. Tołpa, P. Witek, K. Szmuc, E. Kaznowska, M. Osuchowski, P. Król, J. Cebulski, Raman and FTIR spectroscopy in determining the chemical changes in healthy brain tissues and glioblastoma tumor tissues, Spectrochim. Acta A Mol. Biomol. Spectrosc. 225 (2020) 117526. https://doi.org/10.1016/j.saa.2019.117526

[32] M. Kopec, M. Błaszczyk, M. Radek, H. Abramczyk, Raman imaging and statistical methods for analysis various type of human brain tumors and breast cancers, Spectrochim. Acta A Mol. Biomol. Spectrosc. 262 (2021) 120091. https://doi.org/10.1016/j.saa.2021.120091

[33] M. Riva, T. Sciortino, R. Secoli, E. D'Amico, S. Moccia, B. Fernandes, M.C. Nibali, L. Gay, M. Rossi, E. De Momi, L. Bello, Glioma biopsies Classification Using Raman Spectroscopy and Machine Learning Models on Fresh Tissue Samples, Cancers 13 (2021) 1073. https://doi.org/10.3390/cancers13051073

[34] C. Zhang, Y. Han, B. Sun, W. Zhang, S. Liu, J. Liu, H. Lv, G. Zhang, X. Kang, Label-free serum detection based on Raman spectroscopy for the diagnosis and classification of glioma, J. Raman Spectrosc. 51 (2020) 1977–1985. https://doi.org/10.1002/jrs.5931

[35] R. Galli, M. Meinhardt, E. Koch, G. Schackert, G. Steiner, M. Kirsch, O Uckermann, Rapid Label-Free Analysis of Brain Tumor Biopsies by Near Infrared Raman and Fluorescence Spectroscopy—A Study of 209 Patients, Front. Oncol. 9 (2019) 1165. https://doi.org/10.3389/fonc.2019.01165

[36] A. Verma, I. Kumar, N. Verma, P. Aggarwal, R. Ojha, Magnetic resonance spectroscopy — Revisiting the biochemical and molecular milieu of brain tumors, BBA Clin. 5 (2016) 170–178. https://doi.org/10.1016/j.bbacli.2016.04.002

[37] S.K.N. Marie, S.M.O. Shinjo, Metabolism and Brain Cancer, Clinics 66 (2011) 33–43. https://doi.org/10.1590/S1807-59322011001300005

[38] R.I. Ernestus, G. Röhn, R. Schröder, T. Els, Á. Klekner, W. Paschen, N. Klug, Polyamine metabolism in brain tumours: diagnostic relevance of quantitative biochemistry, J. Neurol. Neurosurg. Psychiatry 71 (2001) 88–92. http://dx.doi.org/10.1136/jnnp.71.1.88

[39] B. Delgado-Martín, M.A. Medina, Advances in the Knowledge of the Molecular Biology of Glioblastoma and Its Impact in Patient Diagnosis, Stratification, and Treatment, Adv. Sci. 7 (2020) 1902971. https://doi.org/10.1002/advs.201902971

[40] M. Palani, R. Arunkumar, V.A. Janardhanam, Biochemical and cytogenetic analysis of brain tissues in different grades of glioma patients, Ann. Neurosci. 17 (2010) 120–125.

[41] J.M Cameron, C. Rinaldi, H.J. Butler, M.G. Hegarty, P.M. Brennan, M.D. Jenkinson, K. Syed, K.M. Ashton, T.P. Dawson, D.S. Palmer, M.J. Baker, Stratifying Brain Tumour Histological Sub-Types: The Application of ATR-FTIR Serum Spectroscopy in Secondary Care, Cancers 12 (2020) 1710. https://doi.org/10.3390/cancers12071710

[42] N. Amharref, A. Beljebbar, S. Dukic, L. Venteo, L. Schneider, M. Pluot, R. Vistelle, M. Manfait, Brain tissue characterisation by infrared imaging in a rat glioma model, Biochim. Biophys. Acta 1758 (2006) 892–899. https://doi.org/10.1016/j.bbamem.2006.05.003

[43] T.H. Ali, A. Alhasan, Detection of human brain tumours via evaluation of their biochemical composition using ATR-FTIR spectroscopy, Biomed. Phys. Eng. Express 6 (2019) 015014. https://doi.org/10.1088/2057-1976/ab5cea

[44] T. Hollon, D.A. Orringer, . Label-free brain tumor imaging using Raman-based methods, J. Neurooncol. 151 (2021) 393–402. https://doi.org/10.1007/s11060-019-03380-z

[45] I. Anna, P. Bartosz, P. Lech, A. Halina, Novel strategies of Raman imaging for brain tumor research, Oncotarget 8 (2017) 85290–85310. https://doi.org/10.18632/oncotarget.19668

[46] G. Steiner, A. Shaw, L.P. Choo-Smith, M.H. Abuid, G. Schackert, S. Sobottka, W. Steller, R. Salzer, H.H. Mantsch, Distinguishing and grading human gliomas by IR spectroscopy, Biopolymers 72 (2003) 464–471. https://doi.org/10.1002/bip.10487

[47] A.E. Nikulin, B. Dolenko, T. Bezabeh, R.L. Somorjai, Near-optimal region selection for feature space reduction: novel preprocessing methods for classifying MR spectra, NMR Biomed. 11 (1998) 209–216. https://doi.org/10.1002/(SICI)1099-1492(199806/08)11:4/5<209::AID-NBM510>3.0.CO;2-5

[48] C. Beleites, G. Steiner, M.G. Sowa, R. Baumgartner, S. Sobottka, G. Schackert, R. Salzer, Classification of human gliomas by infrared imaging spectroscopy and chemometric image processing, Vib. Spectrosc. 38 (2005) 143–149. https://doi.org/10.1016/j.vibspec.2005.02.020

[49] S. Koljenović, T.B. Schut, A. Vincent, J.M. Kros, G.J. Puppels, Detection of meningioma in dura mater by Raman spectroscopy, Anal. Chem. 77 (2005) 7958–7965. https://doi.org/10.1021/ac0512599

[50] Y. Zhou, C.H. Liu, Y. Sun, Y. Pu, S. Boydston-White, Y. Liu, R.R. Alfano, Human brain cancer studied by resonance Raman spectroscopy. J. Biomed. Opt. 17 (2012) 116021. https://doi.org/10.1117/1.JBO.17.11.116021

[51] J.R Hands, K.M. Dorling, P. Abel, K.M. Ashton, A. Brodbelt, C. Davis, T. Dawson, M.D. Jenkinson, R.W. Lea, C. Walker, M.J. Baker, Attenuated total reflection fourier transform

infrared (ATR-FTIR) spectral discrimination of brain tumour severity from serum samples, J. Biophotonics 7 (2014) 189–199. https://doi.org/10.1002/jbio.201300149

[52] J.R. Hands, G. Clemens, R. Stables, K. Ashton, A. Brodbelt, C. Davis, T. Dawson, M.D. Jenkinson, R.W. Lea, C. Walker, M.J. Baker, Brain tumour differentiation: rapid stratified serum diagnostics via attenuated total reflection Fourier-transform infrared spectroscopy, J. Neurooncol. 127 (2016) 463–472. https://doi.org/10.1007/s11060-016-2060-x

[53] B.R. Smith, K.M. Ashton, A. Brodbelt, T. Dawson, M.D. Jenkinson, N.T. Hunt, D.S. Palmer, M.J. Baker, Combining random forest and 2D correlation analysis to identify serum spectral signatures for neuro-oncology, Analyst 141 (2016) 3668–3678. https://doi.org/10.1039/C5AN02452H

[54] L.J. Livermore, M. Isabelle, I.M. Bell, C. Scott, J. Walsby-Tickle, J. Gannon, P. Plaha, C. Vallance, P. Ansorge, Rapid intraoperative molecular genetic classification of gliomas using Raman spectroscopy, Neurooncol. Adv. 1 (2019) vdz008. https://doi.org/10.1093/noajnl/vdz008

[55] J.M. Cameron, H.J. Butler, B.R. Smith, M.G. Hegarty, M.D. Jenkinson, K. Syed, P.M. Brennan, K. Ashton, T. Dawson, D.S. Palmer, M.J. Baker, Developing infrared spectroscopic detection for stratifying brain tumour patients: glioblastoma multiforme vs. Lymphoma, Analyst 144 (2019) 6736–6750. https://doi.org/10.1039/C9AN01731C

[56] H.J Butler, P.M. Brennan, J.M. Cameron, D. Finlayson, M.G. Hegarty, M.D. Jenkinson, D.S. Palmer, B.R. Smith, M.J. Baker, Development of high-throughput ATR-FTIR technology for rapid triage of brain cancer, Nat. Commun. 10 (2019) 4501. https://doi.org/10.1038/s41467-019-12527-5

[57] D. Bury, C.L.M. Morais, K.M. Ashton, T.P. Dawson, F.L. Martin, Ex Vivo Raman Spectrochemical Analysis Using a Handheld Probe Demonstrates High Predictive Capability of Brain Tumour Status, Biosensors 9 (2019) 49. https://doi.org/10.3390/bios9020049

[58] J.M. Cameron, J.J.A. Conn, C. Rinaldi, A. Sala, P.M. Brennan, M.D. Jenkinson, H. Caldwell, G. Cinque, K. Syed, H.J. Butler, M.G. Hegarty, D.S. Palmer, M.J. Baker, Interrogation of IDH1 Status in Gliomas by Fourier Transform Infrared Spectroscopy, Cancers 12 (2020) 3682. https://doi.org/10.3390/cancers12123682

[59] C.L.M. Morais, K.M.G. Lima, Comparing unfolded and two-dimensional discriminant analysis and support vector machines for classification of EEM data, Chemometr. Intell. Lab. Syst. 170 (2017) 1–12. https://doi.org/10.1016/j.chemolab.2017.09.001

[60] C.L.M. Morais, P.L. Martin-Hirsch, F.L. Martin, A three-dimensional principal component analysis approach for exploratory analysis of hyperspectral data: identification of ovarian cancer samples based on Raman microspectroscopy imaging of blood plasma, Analyst 144 (2019) 2312–2319. https://doi.org/10.1039/C8AN02031K

[61] R. Bro, A.K. Smilde, Principal component analysis, Anal. Methods 6 (2014) 2812–2831. https://doi.org/10.1039/C3AY41907J

[62] C.L.M. Morais, K.M.G. Lima, Principal Component Analysis with Linear and Quadratic Discriminant Analysis for Identification of Cancer Samples Based on Mass Spectrometry, J. Braz. Chem. Soc. 29 (2018) 472–481. https://doi.org/10.21577/0103-5053.20170159

[63] R.G. Brereton, G.R. Lloyd, Partial least squares discriminant analysis: taking the magic away, J. Chemom. 28 (2014) 213–225. https://doi.org/10.1002/cem.2609

[64] C. Cortes, V. Vapnik, Support-vector networks, Mach. Learn. 20 (1995) 273 –297. https://doi.org/10.1007/BF00994018

[65] C.L.M. Morais, M. Paraskevaidi, L. Cui, N.J. Fullwood, M. Isabelle, K.M.G. Lima, P.L. Martin-Hirsch, H. Sreedhar, J. Trevisan, M.J. Walsh, D. Zhang, Y.G. Zhu, F.L. Martin, Standardization of complex biologically derived spectrochemical datasets, Nat. Protoc. 14 (2019) 1546–1577. https://doi.org/10.1038/s41596-019-0150-x

[66] C.L.M. Morais, M.C.D. Santos, K.M.G. Lima, F.L. Martin, Improving data splitting for classification applications in spectrochemical analyses employing a random-mutation Kennard-Stone algorithm approach, Bioinformatics 35 (2019) 5257–5263. https://doi.org/10.1093/bioinformatics/btz421

Figure Legends

Figure 1: (a) Schematic diagram of Michelson interferometer; (b) the lamellar granting interferometer; (c) dispersive spectrometer.

Figure 2: Stokes and Anti-Stokes Raman scattering, where continuous arrow: absorbed electromagnetic radiation; dashed arrow: released electromagnetic radiation.

Figure 3: (a) IR and (b) Raman biofingerprint regions with their main band assignments. (Reprinted (adapted) with permission from Kelly *et al.*, 2011 [9]. Copyright 2011 American Chemical Society).

Figure 4: Flowchart showing the steps to measure and analyse brain cancer samples. FFPE: formalin-fixed paraffin-embedded, ATR: attenuated total reflection, PCA: principal component analysis, HCA: hierarchical cluster analysis, LDA: linear discriminant analysis, QDA: quadratic discriminant analysis, PLS-DA: partial least squares discriminant analysis, SVM: support vector machines, DBM: difference-between-mean, SPA: successive projections algorithm, GA: genetic algorithm.

Tables

Table 1. Main differences between Raman and IR spectroscopy.

Raman spectroscopy	**Infrared spectroscopy**
It is based on molecular polarizability changes, therefore, only molecules with variation of its polarizability after vibration are Raman active	It is based on changes of molecular dipole moments, therefore, only molecules that change their resultant dipole moment after vibration are IR active
Raman is a scattering technique where the light source is a monochromatic laser not necessarily in the IR region	IR is an absorption technique where the light source emits IR radiation
Raman is water-free	There are several water absorptions in the IR spectrum which may mask the information of interest. Spectra of aqueous samples should be analysed carefully.
Depending on the power or exposure time of the laser light source, Raman may be destructive to the sample [11]	IR is not destructive to the sample

Table 2. Main spectral features in the IR biofingerprint region for brain cancer detection [3].

Wavenumber (cm^{-1})	Assignment	Biomolecule category	Remarks
~950	$\upsilon_s(R-PO_4^{2-})$ of phosphorylated proteins	Proteins	Marker to distinguish brain tumours in tissue [18]
~1030	$\upsilon(C-O/C-C)$ of glycogen	Carbohydrates	Marker to distinguish brain tumours in tissue [18] Marker to distinguish glioma vs. non-glioma samples based on biofluids [27] Marker to distinguish normal vs. brain tumours in biofluids [41]
~1070	$\upsilon(C-C)$	Carbohydrates	Decrease intensity in tumour samples from rat tissue [42]
~1080	$\upsilon_s(PO_2^-)$ of phosphodiester groups	Nucleic acids	Marker to distinguish brain tumours in tissue [23, 43] Increase intensity in brain tumour samples from rat tissue [42] Marker to distinguish glioma vs. non-glioma samples based on biofluids [27] Marker to distinguish normal vs. brain tumours in biofluids [41]
~1155-1172	$\upsilon(C-O)$	Carbohydrates	Shifted in tumour samples from rat tissue [42]
~1225-1236	$\upsilon_{as}(PO_2^-)$ in RNA/DNA	Nucleic acids	Decrease intensity in tumour samples from rat tissue [42] Marker to distinguish brain tumour tissue [18, 43] Marker to distinguish normal vs. brain tumours in biofluids [41]
~1260	Amide III: $\upsilon(C-N)$	Proteins	Marker to distinguish brain tumour tissue [18] Marker to distinguish normal vs. brain tumours in biofluids [41] Marker to distinguish glioma vs. non-glioma samples based on biofluids [27]
~1380-1394	$\delta(CH)$	Lipids/Proteins	Marker to distinguish normal and tumour tissue [41] Marker to distinguish normal vs. brain tumours in biofluids [41]
~1550	Amide II: $\delta(N-H)$ coupled to $\upsilon(C-N)$	Proteins	Marker to distinguish glioma vs. non-glioma samples based on biofluids [27] Marker to distinguish normal and tumour tissue [41] Marker to distinguish normal vs. brain tumours in biofluids [41]
~1650	Amide I: $\upsilon(C=O)$	Proteins	Marker to distinguish glioma vs. non-glioma samples based on biofluids [27] Marker to distinguish normal and tumour tissue [41] Marker to distinguish normal vs. brain tumours in biofluids [41]
~1740	$\upsilon(C=0)$	Lipids	Band become weak and even disappearing in tumour samples from tissue [42] Marker to distinguish normal vs. brain tumours in biofluids [41]
~1750	$\upsilon(C=C)$	Lipids	Marker to distinguish brain tumour tissue [43]

υ = stretching; υ_s = symmetric stretching; υ_{as} = asymmetric stretching; δ = bending

Table 3. Main spectral features in the Raman biofingerprint region for brain cancer detection [12].

Wavenumber (cm^{-1})	Assignment	Biomolecule category	Remarks
~498	$\upsilon(C-O)$ glycogen	Carbohydrates	Marker for IDH-mutant glioma [44]
~524	$\upsilon(S-S)$	Proteins	Marker for glioma tissue [33]
~725	Ring breathing mode of DNA/RNA bases	Nucleic acids	Marker for brain tumours [45]
~750	$\delta(CH)$ out-of-plane	Nucleic acids	Marker for brain tumours [32]
~826	$\upsilon(O-P-O)$ DNA	Nucleic acids	Marker for IDH-mutant glioma [44] Marker for glioma tissue [33]
~875	$\upsilon(N^+-CH_3)$ phospholipids	Lipids	Marker for glioma tissue [33]
~911	$\upsilon(C-C)$ glucose	Carbohydrate	Marker for meningioma tissue [18]
~956	$\upsilon(C-O)$ collagen	Proteins	Marker for brain tumours [32, 45]
~960	$\upsilon(PO_4^{3-})$ Hydroxyapatite	Mineral	Marker for brain tumours [35]
~1004	$\upsilon_s(C-C)$ ring breathing of phenylalanine in collagen	Proteins	Marker for IDH-mutant glioma [44] Marker for brain tumours [32, 35, 45]
~1064	$\upsilon(C-C)$ skeletal model	Lipids	Marker for brain tumours [45]
~1080-1158	$\upsilon_s(P=O)$ nucleic acids and phospholipids	Lipids/Nucleic acids	Marker for brain tumours [45] Marker for brain tumours [35]
~1126	$\upsilon(C-C)$ skeletal of acyl backbone	Lipids	Marker for brain tumours [32]
~1156	$\upsilon(C-C)$ carotenoids	Pigment	Marker for brain tumours [32, 35] Absent in normal tissue [12]
~1174	$\delta(C-H)$	Proteins	Marker for IDH-mutant glioma [44]
~1200–1350	Amide III: $\upsilon(C-N)$	Proteins	Marker for brain tumours [18, 32, 35, 45]
~1307	$\delta(CH_2/CH_3)$ collagen or lipids	Proteins/Lipids	Marker for brain tumours [32]
~1337	$\delta(CH_2/CH_3)$	Lipids	Marker for IDH-mutant glioma [44]
~1444	$\delta(CH_2)$ fatty acids	Lipids	Marker for IDH-mutant glioma [44] Marker for brain tumours [35, 45]
~1480–1575	Amide II: $\delta(N-H)$ coupled to $\upsilon(C-N)$	Proteins	Marker for brain tumours [45]
~1520	$\upsilon(C=C)$ carotenoids	Pigment	Marker for brain tumours [32] Absent in normal tissue [12] Marker for brain tumours [35]
~1585	$\upsilon(C=C)$ olefin	proteins	Marker for brain tumours [32]
~1600–1800	Amide I: $\upsilon(C=O)$	Proteins	Marker for brain tumours [18, 35, 45]
~1655	$\upsilon(C=C)$ fatty acids	Lipids	Marker for brain tumours [32 ,45]

υ = stretching; υ_s = symmetric stretching; υ_{as} = asymmetric stretching; δ = bending

Table 4. Overview of FT-IR and Raman studies to investigate brain cancers.

Technique	Sample type	Samples	Algorithm	Main results	Reference
FT-IR (Imaging)	Tissue (snap-frozen)	Non-cancer control Astrocytoma grade III Astrocytoma grade II Glioblastoma	GA-LDA	Sample discrimination at 89% accuracy	Steiner *et al.* (2003) [46]
FT-IR (Imaging)	Tissue (snap-frozen)	Non-cancer control Glioblastoma grade IV Astrocytoma grade III Astrocytoma grade II	ga_ors [47]	Samples groups classified at 64% overall accuracy. Control tissues classified at 95% accuracy.	Beleites *et al.* (2005) [48]
Raman (Mapping)	Tissue (snap-frozen)	Normal dura mater Meningioma	LDA PLS-DA	100% discrimination between normal and meningioma	Koljenović *et al.* (2005) [49]
Raman (Resonance)	Tissue (snap-frozen)	Meningiomas Normal tissue Glioblastoma Acoustic neuroma Pituitary adenoma	PCA-SVM	90.9% sensitivity and 100% specificity to discriminate the samples	Zhou *et al.* (2012) [50]
FT-IR (ATR-FTIR) Raman	Tissue (FFPE)	Normal brain Meningioma Glioma Brain metastases LA AA GBM	LDA PCA-LDA	Statistically significant differences were found between the samples groups and subgroups	Gajjar *et al.* (2013) [18]
FT-IR (ATR-FTIR)	Serum	Non-cancer control Glioma (HGG, LGG)	SVM	Discrimination of non-cancer vs. gliomas with an average sensitivity of 93.75%, and average specificity of 96.53%	Hands *et al.* (2014) [51]
FT-IR (ATR-FTIR)	Serum	Non-cancer control Brain cancer Metastatic cancer Glioma (HGG, LGG) Meningioma	SVM	Samples groups and subgroups were classified with accuracies between 80-100%	Hands *et al.* (2016) [52]
FT-IR (ATR-FTIR)	Serum	Non-cancer control Brain cancers	Random forest	Samples discriminated at 92.8% sensitivity	Smith *et al.* (2016) [53]

			2D correlation analysis	and 91.5% specificity.	
Raman	Serum	Non-cancer control Meningiomas	PCA-LDA	Sample discrimination at 80% sensitivity and 92% specificity	Mehta *et al.* (2018) [20]
Raman	Tissue (fresh, snap-frozen, FFPE)	Astrocytoma IDH-wildtype IDH-mutant Oligodendroglioma	PCA-LDA	79%-94% sensitivity and 90-100% specificity to classify glioma subtypes and 91% sensitivity and 95% specificity to classify IDH mutation.	Livermore *et al.* (2019) [54]
FT-IR (ATR-FTIR)	Serum	Non-cancer control Brain cancers	PLS-DA SVM Random forest	Non-cancer vs. cancer discrimination at 91% sensitivity and specificity. Glioblastoma vs. lymphoma discrimination at 90.1% sensitivity and 86.3% specificity.	Cameron *et al.* (2019) [55]
FT-IR (ATR-FTIR)	Serum	Non-cancer control Brain cancers	SVM	Sample discrimination at 93.2% sensitivity and 92.8% specificity	Butler *et al.* (2019) [56]
Raman (Imaging)	Tissue (FFPE)	Meningioma grade I Meningioma grade II	PCA-QDA SPA-QDA	Sample discrimination at 96.2% accuracy (85.7% sensitivity and 100% specificity)	Morais *et al.* (2019) [10]
Raman (Handheld)	Tissue (FFPE, fresh)	Normal brain LGG HGG Meningiomas Metastases Lymphoma	PCA-LDC	Samples groups were discriminated at 90.3–99.6% accuracies (fresh tissue) and 88.0–99.5% accuracies (FFPE)	Bury *et al.* (2019) [57]

FT-IR (ATR-FTIR)	Plasma	Normal brain HGG LGG Meningioma Brain metastases	PCA-LDC SVM	Discrimination between normal vs. LGG vs. HGG at 100% accuracy Discrimination between all groups at 97% accuracy	Bury *et al.* (2019) [23]
FT-IR (ATR-FTIR) Raman	Tissue (fresh-frozen)	Normal brain Glioma Meningioma	PCA-QDA GA-QDA	Non-tumour *vs.* tumour were correct classified at 94% (Raman) and 97.2% (FT-IR)	Bury *et al.* (2020) [16]
FT-IR (ATR-FTIR)	Tissue (FFPE)	Meningioma grade I Meningioma grade II Meningioma grade I from Recurrence	PLS-DA	79% accuracy (grade I vs. grade II) 94% accuracy (grade I vs. grade I from recurrence) 97% accuracy (grade II vs. grade I from recurrence)	Lilo *et al.* (2020) [21]
FT-IR (ATR-FTIR, Synchrotron)	Serum Tissue	Gliomas (IDH1 mutated and wild-type)	LDA PLS-DA	Discrimination of IDH1 samples using serum at 69.1% accuracy; and, using tissue at 82.9% accuracy	Cameron *et al.* (2020) [58]
FT-IR (ATR-FTIR)	Serum	Non-cancer control Glioblastoma Meningioma Lymphoma Metastasis	PLS-DA SVM Random forest	Discrimination between controls vs. brain cancers at sensitivity and specificity above 90%. Discrimination brain lesions with accuracies above 80%.	Cameron *et al.* (2020) [41]

ATR-FTIR: attenuated total reflection Fourier-transform infrared spectroscopy. FFPE: formalin-fixed paraffin-embedded. LA: low-grade astrocytoma. AA: anaplastic astrocytoma. GBM: lioblastoma multiforme. HGG: high-greade glioma. LGG: low-grade glioma. GA-LDA: genetic algorithm linear discriminant analysis. LDA: linear discriminant analysis. PLS-DA: partial least squares discriminant analysis. PCA-LDA: principal component analysis linear discriminant analysis. PCA-SVM: principal component analysis support vector machines. SVM: support vector machines. PCA-QDA: principal component analysis quadratic discriminant analysis. SPA-QDA: successive projections algorithm quadratic discriminant analysis. PCA-LDC: principal component analysis linear discriminant classifier. GA-QDA: genetic algorithm quadratic discriminant analysis.

Figures

Figure 1

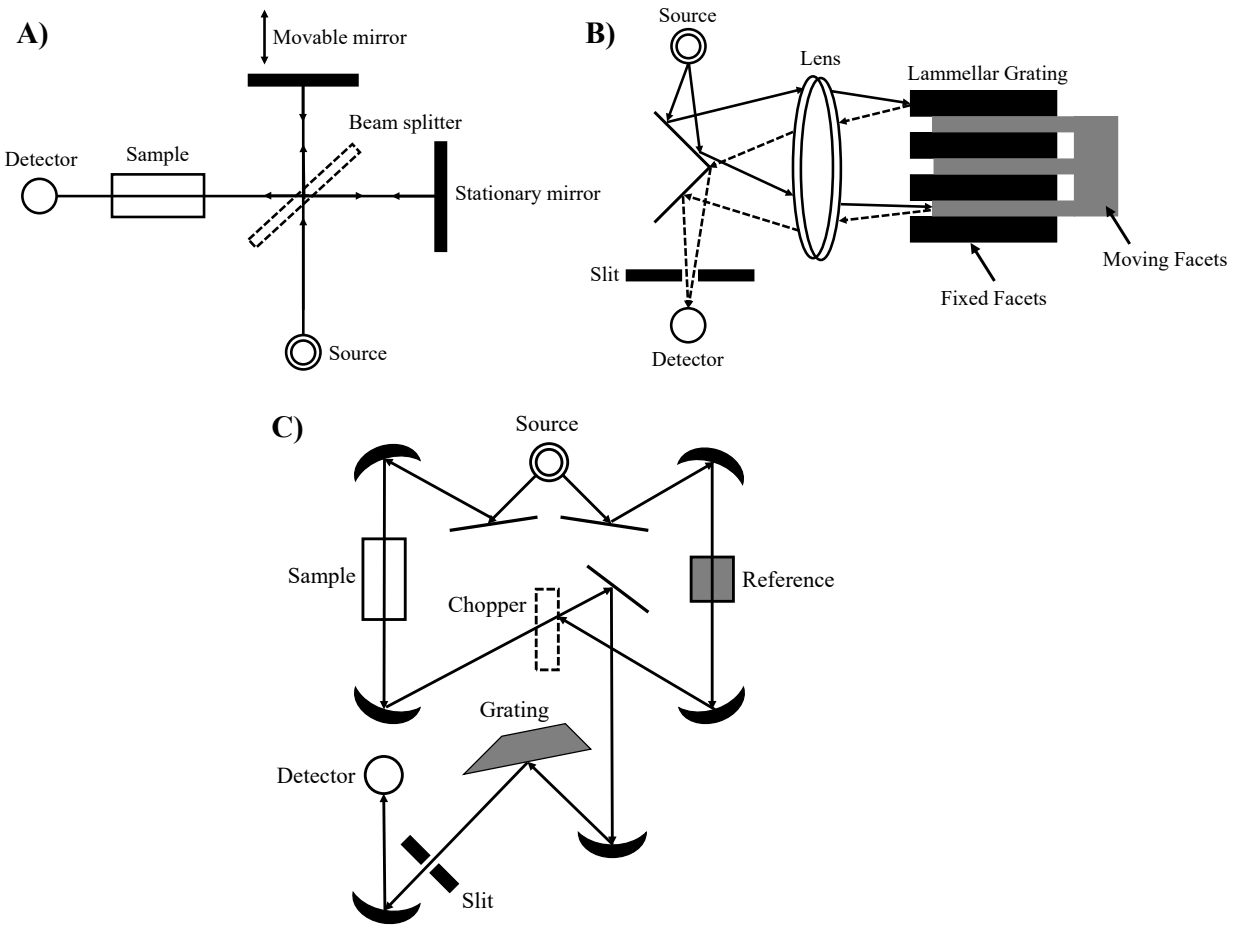
A)
Movable mirror
Beam splitter
Detector
Sample
Stationary mirror
Source
B)
Source
Lens
Lammellar Grating
Slit
Moving Facets
Fixed Facets
Detector
C)
Source
Sample
Reference
Chopper
Grating
Detector
Slit

Figure 2

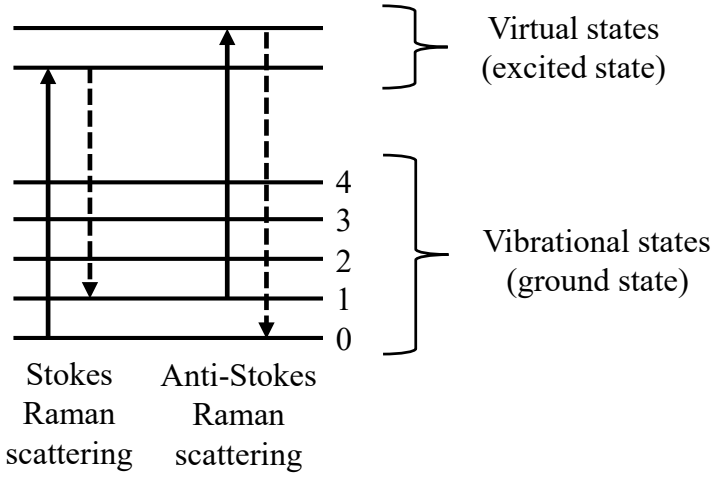
Virtual states
(excited state)
4
3
2
1
0
Vibrational states
(ground state)
Stokes
Raman
scattering
Anti-Stokes
Raman
scattering

Figure 3

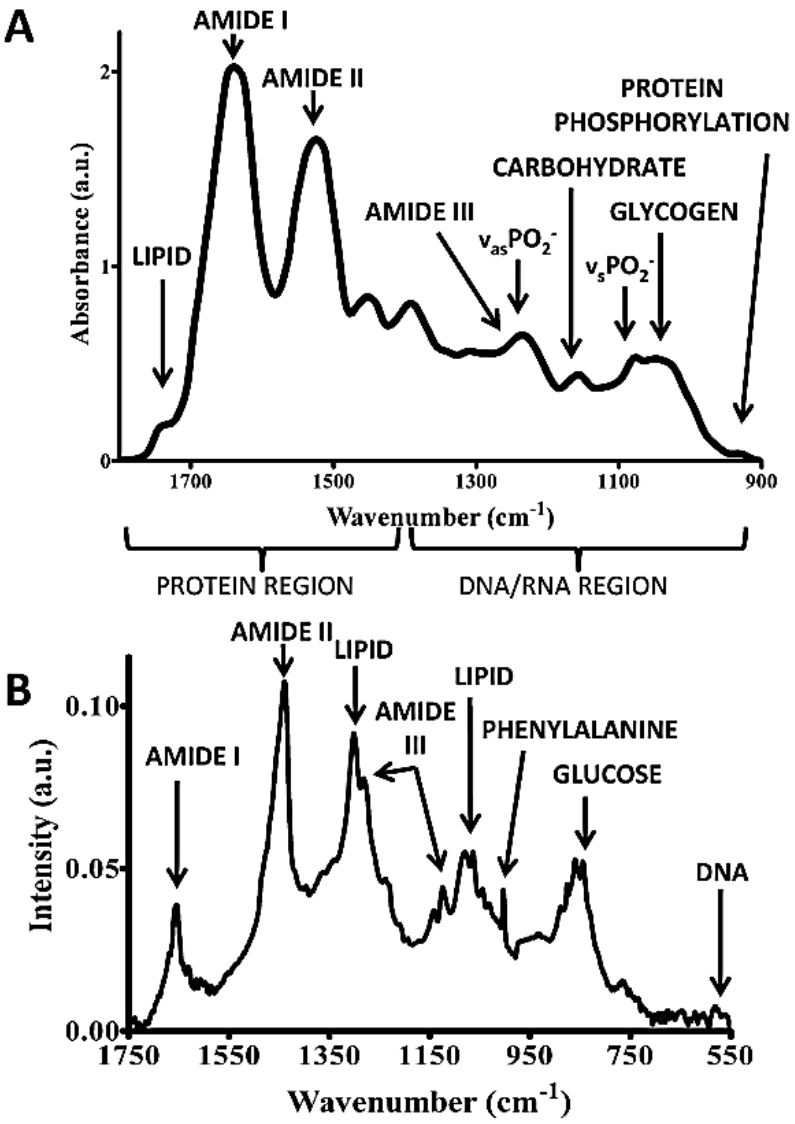
A
AMIDE I
AMIDE II
PROTEIN
PHOSPHORYLATION
CARBOHYDRATE
GLYCOGEN
AMIDE III
$\nu_{as}PO_2^-$
$\nu_sPO_2^-$
LIPID
Absorbance (a.u.)
2
1
0
1700
1500
1300
1100
900
Wavenumber (cm^{-1})
PROTEIN REGION
DNA/RNA REGION
B
AMIDE II
LIPID
LIPID
AMIDE
III
PHENYLALANINE
GLUCOSE
AMIDE I
DNA
Intensity (a.u.)
0.10
0.05
0.00
1750
1550
1350
1150
950
750
550
Wavenumber (cm^{-1})

Figure 4

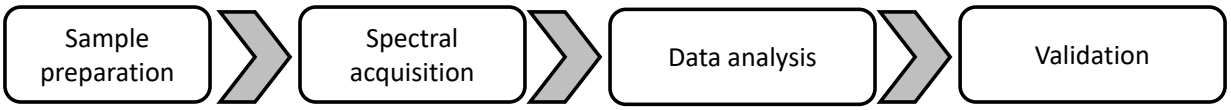

- Sample type: biofluid or tissue.
- Biofluid preparation: unthawing, drying, centrifugation, etc.
- Tissue preparation: fresh, snap-frozen, FFPE, etc.

- Acquisition mode: transmittance, reflectance, ATR, microscopy, imaging.
- Spectral resolution.
- Wavenumber range
- Raman: laser source wavenumber, power, exposure time, aperture.
- Raman filters: fluorescence, saturation, cosmic rays.
- File extension format.

- Pre-processing.
- Exploratory analysis: PCA, HCA.
- Sample splitting.
- Classification: LDA, QDA, PLS-DA, SVM.
- Feature extraction and selection: DBM spectra, PCA loadings, PLS-DA, SPA, GA.

- Cross-validation.
- Blind prediction of test samples.
- Calculation of quality parameters: accuracy, sensitivity, specificity, etc.
- Confusion matrices.
- Statistical test for the key spectral features.